SPECIAL ISSUE ARTICLE



Check for updates

Exploring fracture anisotropy in tantalum carbide compounds: A density functional theory approach

Sajjad Hossain¹ 🕟 📗 Gregory B. Thompson² 📗 Christopher R. Weinberger^{1,3} 📵

Correspondence

Christopher R. Weinberger, School of Advanced Materials Discovery, Colorado State University, Fort Collins, CO 80523, USA.

Email: Chris.Weinberger@colostate.edu

Funding information

National Science Foundation: Directorate for Mathematical and Physical Sciences, Grant/Award Numbers: 2323456, 2323458

Abstract

In this paper, we examine the cleavage fracture anisotropy in tantalum carbides, namely, TaC, α -Ta₂C, and ζ -Ta₄C_{3-x}, using density functional theory (DFT) calculations. Our investigation identifies the presence of multiple low-energy cleavage planes indicating multiple potential pathways for crack propagation in these ceramics, even the low symmetry compounds. The anisotropy characteristics of cleavage fractures exhibited by α -Ta₂C and ζ -Ta₄C_{3-x} closely align with the intrinsic fracture anisotropy observed in TaC. Notably, there exist at least three pyramidal planes in ζ -Ta₄C_{3-x} whose cleavage energies are less than those of the carbon-depleted basal planes, previously reported to have the lowest cleavage energy. The observed preference in experiments for cleavage along carbon-depleted basal planes, exclusive of other identified low-energy planes, points to factors beyond cleavage energy influencing cleavage plane preference.

KEYWORDS

carbides, cleavage planes, density functional theory, fracture, zeta phase

1 | INTRODUCTION

Tantalum carbides, which are part of the ultra-high temperature ceramic family that is characterized by their high melting temperatures and hardness, have drawn heightened scientific focus for their enhanced low-temperature fracture toughness. This high toughness is credited to the presence of the zeta (ζ -Ta₄C_{3-x}) phase; thereby, enhancing their thermomechanical application scope. ^{1–10} The fracture toughness of these carbides is dependent on the carbon content and the volume fraction of the zeta phase and ranges from 2 to 15 MPa $\sqrt{\rm m}$. ^{8,9} Specifically, carbonto-tantalum ratios (C/Ta) of 0.8–1.0 are linked to modest toughness values of 4–6 MPa $\sqrt{\rm m}$, corresponding to stoichiometric and substoichiometric cubic γ -TaC. ^{5,8,11–13}

Trigonal α -Ta₂C, which has a carbon-to-tantalum ratio of 0.5, has a fracture toughness of 6–9 MPa \sqrt{m} . 5.8,9,14,15 Conversely, in compositions where the C/Ta ratio lies between 0.6 and 0.8, the material has a two-phase microstructure consisting of γ -TaC and ζ -Ta₄C_{3-x} or α -Ta₂C and ζ -Ta₄C_{3-x}, where the ζ -Ta₄C_{3-x} phase constitutes 12%–80% of the overall volume. The toughness values of these materials are found to range between 11 and 15 MPa \sqrt{m} , with higher volume fractions of ζ -Ta₄C_{3-x} resulting in higher fracture toughness. 5–7 This notable increase in fracture toughness is believed to stem from microstructural toughening mechanisms linked to the "lath" or plate-like microstructure. 5,16–21 The exact contributions of different toughening mechanisms remain unquantified, underscoring the need for a deeper understanding of the fracture

This is an open access article under the terms of the Creative Commons Attribution-NonCommercial License, which permits use, distribution and reproduction in any medium, provided the original work is properly cited and is not used for commercial purposes.

© 2024 The Author(s). Journal of the American Ceramic Society published by Wiley Periodicals LLC on behalf of American Ceramic Society.

¹School of Advanced Materials Discovery, Colorado State University, Fort Collins, Colorado, USA

²Department of Metallurgical and Materials Engineering, University of Alabama, Tuscaloosa, Alabama, USA

³Department of Mechanical Engineering, Colorado State University, Fort Collins, Colorado, USA



mechanics in tantalum carbides as a representative of the hard metals.

Since the high fracture toughness in the presence of the zeta phase is postulated to be due to microstructure, it is important to note that how the individual ceramic phases fracture. However, most investigations into the fracture of tantalum carbides focus toughening the materials rather than reporting details of the fracture process. 6,8,22-27 The limited direct observations of fracture single crystal γ -TaC indicate that the fracture predominantly occurs along the {100} plane. The preferences for intergranular and transgranular fracture have both been noted, 13,28 however, extensive studies have not clarified what controls this choice, though porosity and carbon content likely play a role. The preference for {100} cleavage, however, is also reported in the fracture of polycrystalline materials. 11-13 This inclination toward cleavage on these planes is further supported by first-principles studies, 10,29 which have identified the {100} plane as having the lowest cleavage energy in B1 γ -TaC. In contrast, the α -phase of tantalum hemicarbide (α-Ta₂C) adopts a trigonal C6 structure, where tantalum atoms form a hexagonal close-packed sublattice and carbon atoms selectively fill every other layer of octahedral sites along the (0001) resulting in alternating carbon-rich and carbon-depleted layer stacking sequence. 18-20,30 The fracture behavior of single crystalline α -Ta₂C, including its preferred cleavage planes, is unexplored. Polycrystalline α -Ta₂C shows both intergranular fracture, ^{14,15} and transgranular fracture, 15 the transition appears related to porosity with higher porosity favoring intergranular. The morphology of elongated Ta₂C grains is thought to be a key factor in determining the path of fracture propagation, significantly enhancing fracture toughness. 31,32 Cracks often exhibit a tendency to deviate or twist around elongated, rod-like grains, a phenomenon described as "discontinuous brittle reinforcements,"14,32 which can be interpreted as a form crack deflection and grain bridging. Such reinforcements, combined with plate-like matrix grains or second-phase platelets, align with the observed lamellar microstructure in the rhombohedral ζ -phase. ^{14,33}

The ζ -phase exhibits a distinctive "lath" or plate-like lamellar microstructure which can be interpreted as the laths or grains being foreshortened along the $\langle 0001 \rangle$ direction and elongated along directions perpendicular to it.^{5,16–21} Experimental studies have shown a tendency for cracks within the zeta phase to propagate along these laths and thus along $\{0001\}$ planes^{5,9}; which are interpreted to be carbon-depleted interfaces between Ta–Ta $\{0001\}$ basal planes and thus behave as "weak interfaces." Density functional theory (DFT) calculations^{10,29} support this observation, indicating that Ta–Ta bonded basal planes are more susceptible to cleavage than Ta–C bonded ones, with carbon-depleted $\{0001\}$ planes in ζ -Ta₄C_{3-x} being

favorable paths for crack propagation according to Griffith's criterion. This is further evidenced by Sygnatowicz et al.'s observation of rising R-curve fracture behavior in these materials, demonstrating a microstructural toughening mechanism in the zeta phase. These findings highlight the critical role of microstructure, particularly in the presence of the ζ -Ta₄C_{3-x}, in contributing to the remarkable fracture toughness observed in these ceramics. 5.8-10,18,19,29

The nanoscale "lath" microstructures in the zeta phase $(\zeta$ -Ta₄C_{3 - x}) typically precipitate from a parent matrix during processing, which is either γ -TaC or α -Ta₂C. ^{10,29} Upon precipitation, the $\{0001\}$ (basal) planes of the ζ -Ta₄C_{3-x} phase are found be parallel to the close-packed planes of either γ -TaC {111} or α -Ta₂C {0001}. This alignment is a result of the minimal interfacial energy between the zeta and matrix phases associated with this orientation relationship.³⁵ When α -Ta₂C serves as the matrix phase, the laths tend to exhibit a parallel lamellar structure. In contrast, when γ -TaC is the matrix phase, the laths display a crisscross microstructure. 5,16,18 This can be attributed to the variance in available planes in the matrix phase; γ -TaC has four equivalent {111} planes misoriented by 70.5°, while α -Ta₂C has an only one {0001} plane orientation. The high fracture toughness had been observed irrespective of the matrix phase.6-9

The two different microstructures of the TaC-Ta₄C_{3-x} and Ta₂C-Ta₄C_{3-x} two-phase materials arise from the crystal structures of the constituent phases. The precipitation of ζ -Ta₄C_{3-x} from the B1 structure involves the removal of every fourth carbon layer and subsequent shearing, resulting in a transformation that respects the grain orientation of the original matrix—γ-TaC.³⁵ The stacking sequence of γ -TaC along the $\langle 111 \rangle$ direction can be denoted as: ... A γ B α C β ... where A, B, and C represent the stacking sequence of Ta atoms while α , β , and γ represent the stacking of the carbon atoms. Removal of carbon layers from this sequence triggers an energetically favorable shearing process.³⁵ This adjustment disrupts the regular stacking order, resulting in the formation of stacking faults. The stacking sequence of atomic planes in rhombohedral ζ -Ta₄C_{3-x} can be written as: ... A γ B | A γ $B \alpha C \beta A | C \beta A \gamma B \alpha C | B \alpha C \beta ... and ... A \gamma B | ... for \alpha$ Ta₂C^{4,18,19,36}; where | signifies a carbon-depleted stacking fault relative to the B1 structure. Thus, it is clear that the zeta phase can be obtained from γ -TaC by coupled carbon depletion and shearing of every fourth layer while the zeta phase can be obtained from α -Ta₂C by shearing and filling every other carbon depleted layer. These transformation pathways, along with an essentially zero interfacial energy³⁵ explain the observed orientation relationships in tantalum carbides that have the zeta phase. 16,17,37,38

The aforementioned discussion of orientation relationships among the tantalum carbides would suggest the composition of ζ -Ta₄C_{3-x} is TaC_{0.75}. ^{17,18} However, experimental work ^{33,39-41} has demonstrated that its homogeneity ranges between TaC_{0.62} to TaC_{0.68} and with the structure of the metal atoms determined by Yvon and Parthé⁴² and later confirmed by Martin et al. ⁴³ and Gusev et al. ⁴¹ with an assigned space group of $R\bar{3}m$. DFT investigations by Weinberger and Thompson ¹⁹ have confirmed the thermodynamic stability of the zeta phase, confirmed the metal ordering, and established the carbon structural vacancy ordering in agreement with the available experimental results ^{39,41,44} as well as its standard chemistry: ζ -Ta₃C₂.

Bonding and microstructure are instrumental in dictating toughening mechanisms in materials, tantalum carbides being no exception.5,9,29 While the lath microstructure of ζ -Ta₄C_{3-x} is considered an important factor in toughness improvement, the presence of a similar β -Nb₂C lath-like structure in niobium carbides, without enhanced toughness, suggests that the lath morphology is not the sole determinant.⁴⁵ Distinct from β -Nb₂C, ζ -Ta₄C_{3-x} showcases alternating face centered cubic/hexagonal closed packed (fcc/hcp) stacking sequences and carbon-depleted stacking faults, which are the preferential cleavage planes. In contrast, β -Nb₂C's uniform carbon ordering might limit its fracture pathways by creating more uniform cleavage energy across crystallographic planes. The platelet-like microstructure consisting of localized metal-metal bonded low-energy cleavage planes {0001} seems to be the prerequisite for rising toughness in the tantalum carbide ceramics.⁴⁵ The crisscrossed and short grains in ζ -Ta₄C_{3-x} facilitate a complex crack path, enhancing toughness through mechanisms like crack deflection and bridging.⁵ As cracks in these materials typically propagate parallel to the laths, when perpendicular, the laths deflect the cracks, resulting in varied crack lengths and anisotropic fracture behavior that increases toughness. Additionally, long cracks may be deflected around unfavorably oriented laths, further enhancing toughness through grain or lamella bridging. 5,9,19 Similar toughening mechanism effects were noted in TaC reinforced with graphene nanoplatelets. 46 The random orientation of these platelets within the TaC matrix produced a similarly intricate crack path, culminating in toughness levels around 11 MPa \sqrt{m} .⁴⁶ The bending, sliding, and kinking have also been seen in those graphene nanoplatelets as energy dissipation mechanisms.46 Schwind et al. observed similar kinking/buckling and delamination in ζ -Ta₄C_{3-x} samples at elevated temperatures.⁷

Such observations raise pivotal questions about the primary toughening mechanisms in tantalum carbides, particularly in the context of grain bridging. The effectiveness of grain bridging, a process contingent on the existence

of a limited number of easy cleavage planes, hinges on whether the Ta–Ta {0001} basal plane in the zeta phase possesses the lowest cleavage energy. This raises the question of whether there are additional planes in ζ -Ta₄C_{3 - x} that might exhibit lower cleavage energies. Such comparison is crucial for understanding the microstructural attributes and fracture behavior in tantalum carbides. In this paper, we investigate the cleavage energy of different planes in tantalum carbides to fully determine if these materials truly have anisotropic cleavage properties. By simulating cleavage along distinctive planes of these compounds, we aim to gain insights into the fracture anisotropy which is going to elucidate a fundamental understanding of brittle fracture propagation in tantalum carbides.

2 | METHODS

The Vienna Ab initio Simulation Package (VASP) was used to perform DFT calculations at zero Kelvin to compute the cleavage energies. 47-50 Projector-augmented wave pseudopotentials⁵¹ and a plane wave basis⁴⁹ were utilized in the simulations. The generalized gradient approximation (GGA) utilizing the parameterization of Perdew-Burke-Ernzerhof (PBE) was chosen for the evaluation of exchange-correlation energies⁵² with additional limited simulations utilizing the local density approximation (LDA). For k-space integration, the Monkhorst-Pack method was employed with $11 \times 11 \times 11$ integration points for the conventional eight atom B1 TaC unit cell, characterized by a 4.47 Å lattice constant. In subsequent simulations, this configuration was proportionally adjusted to maintain nearly uniform density (K-point density of 2π * 0.04 Å^- ź) in the reciprocal space. A plane wave cutoff energy of 600 eV ensured converged results. The valence electrons used for the simulation of tantalum carbides are (Ta: 5d36s2) and (C: 2s22p2). The tolerance for electronic structure calculations was set at 1×10^{-6} eV and structural relaxation tolerance was set to 1×10^{-5} eV; structural relaxations with a force tolerance of 0.01 eV/Å did not alter the results. All data required to reproduce the results in this paper can be found in the supporting information, Tables S1–S7.

For DFT simulations of cleavage fracture along a predetermined plane, a supercell mimicking the host crystal was created, extending along the normal of the cleavage plane of interest. A separation gap measuring 10 Å was introduced to obtain the value of converged cleavage energy. The cleavage energy, γ , was determined using the equation: $\gamma = \frac{E-E_0}{A}$ where A is the area of the plane, E is the energy of the cleaved crystal, and E_0 is the energy of the intact crystal. As illustrated in Figure 1, the cleavage energy

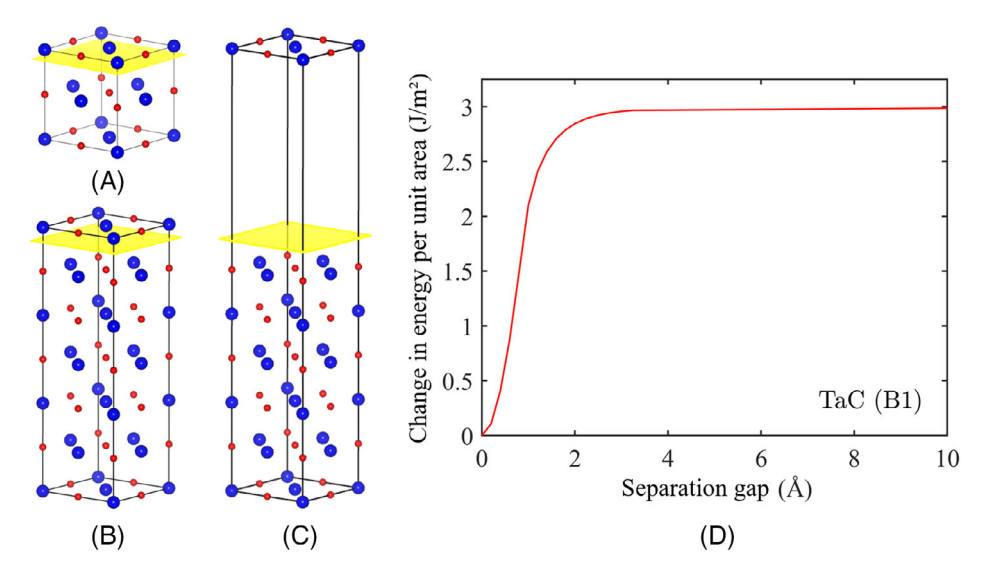


FIGURE 1 A representative simulation methodology to determine the cleavage energy with the $\{100\}$ plane in the B1 rocksalt structure of tantalum carbide. (A) A unit cell of B1 TaC, (B) a $1 \times 1 \times 3$ supercell of the B1 TaC unit cell, (B) the structure after the introduction of a 10 Å gap, and (C) the variation of the system energy per unit surface area with respect to the separation gap; the cleavage energy is the converged value.

monotonically increases as separation gap increases and it converges to a certain value. This figure is comprised: (a) a unit cell of B1 TaC, (b) the pristine supercell prior to cleavage, (c) the modified supercell post gap introduction, and (d) an example of the system energy plotted as a function of the separation gap. The graph delineates a characteristic rise and stabilization of the energy with increasing separation, converging to the cleavage energy at large separation; here the cleavage energy is that of a {100} plane of B1 rocksalt tantalum carbide. Since the directions in the plane of cleavage are periodic, the smallest repeat in these directions was always used. However, cleavage breaks symmetry in the direction normal to the plane as it may have a size dependence. To examine this in all our simulations, we created supercells that are $1 \times 1 \times N$ with variable N and computed the cleavage energy as a function of N. As an example, the energy variation of the cleavage energy of the {100} plane for N > 1 is less than 0.01 J/m². This demonstrates relatively quick convergence of the cleavage energy. The variation is consistent with previous studies of the cleavage and surface energies in this system.²⁹

3 | RESULTS AND DISCUSSION

3.1 | Fracture along different cleavage planes in TaC

As noted previously, the BI rocksalt TaC, the crystal cleaves on {100} planes in experiments and DFT suggests that the {100} planes have the lowest cleavage energy followed by the {110} and {111} (Figure 2). To demonstrate consistency with previous results, we computed the cleavage energies

of these low indices planes. As illustrated in Figure 3, the cleavage energy for the $\{100\}$ plane is 2.98 J/m², for $\{110\}$ plane is measured at 6.48 J/m², and the $\{111\}$ plane, being the most robust against cleavage, is observed at 8.21 J/m². This indeed comports with previous findings of the cleavage energy in these materials. 10,29,53,54

To demonstrate that these are indeed the lowest cleavage energy and to examine how the cleavage energy varies, we computed the cleavage energy of a series of planes between the $\{100\}$ and $\{110\}$, Figure 3A, as well as between the $\{100\}$ and $\{111\}$, Figure 3B. The energy increases as the angle (φ) between the $\{100\}$ plane and the other planes is increased as shown in Figure 3C. Thus, the cleavage energies follow the sequences: $\{100\} < \{014\} < \{012\} < \{034\} < \{011\}$, and $\{100\} < \{114\} < \{112\} < \{334\} < \{111\}$.

Figure 3C shows cleavage energy as a function of the angle between the plane and the {100} plane. It is interesting to note that the cleavage energy varies roughly linearly with angle. Perhaps more notable, however, is there is no strong evidence of cusps (local minima and maxima) in the cleavage energy, which is frequently observed in surface energies^{55–57} and grain boundary energies.^{58–60}

Yu et al.²⁹ suggested that while stoichiometric B1 TaC favors the {100} plane cleavage, carbon depletion shifts this preference to the {111} planes, thus altering the favored fracture pathway. In pursuit of a deeper understanding of this phenomenon, we performed the cleavage energy simulations for both {100} and {111} planes under varying degrees of carbon content. By methodically adjusting the carbon-to-tantalum (C/Ta) ratio within these planes, we have simulated scenarios ranging from stoichiometric to significantly carbon-depleted environments.

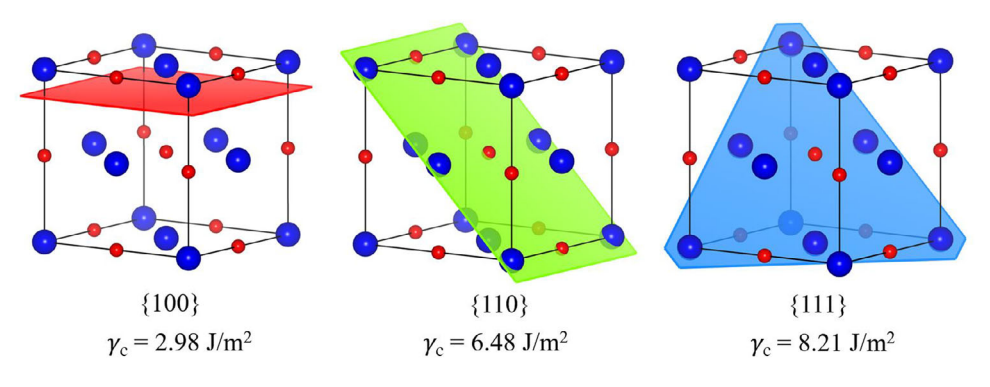


FIGURE 2 The cleavage planes and energy of the {100}, {110}, and {111} planes in the TaC rocksalt structure.

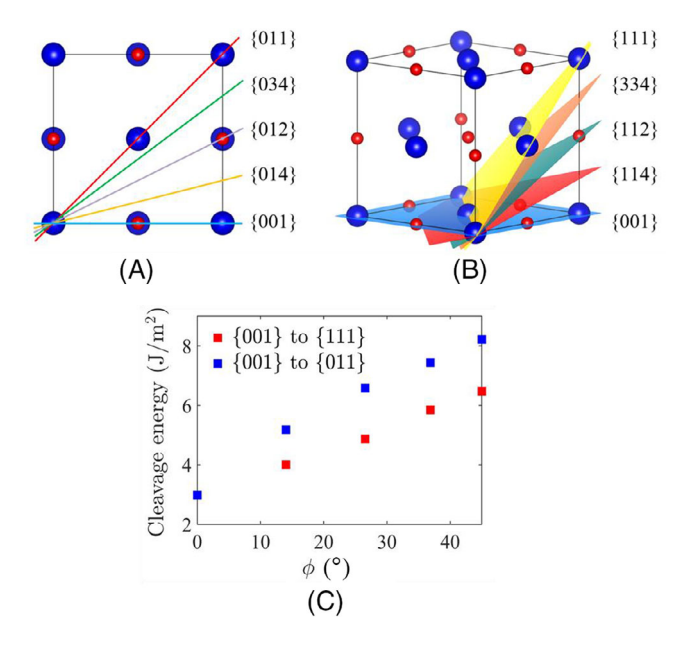


FIGURE 3 The cleavage energies of the planes between the {100} and (A) {011} and (B) {111} planes in the B1 rocksalt structure of TaC (C) are plotted as a function of the angle between the plane and the {100}.

The carbon was removed from each specific plane, an example of how this was done is shown in Figure 4A,B for the {100} plane and the cleavage energy of this specific plane was evaluated. Figure 4C,D shows the change in cleavage energy as carbon is removed from the {100} and {111} planes in B1 TaC. As the C/Ta ratio decreases for the {100} surface, the cleavage energy increases, indicating an indirect and nearly linear relationship between cleavage energy and carbon concentration. Conversely, the cleavage energy of {111} plane has a nearly linear direct relationship with carbon concentration. Thus, we observe the same trends as Yu et al.²⁹ in that the {100} surface increases in cleavage with carbon loss while the {111} surface has a reduction in cleavage energy with carbon loss.

Figure 4E shows the cleavage energy of all three planes fully carbon filled (red line) and fully carbon depleted (black line). As has been previously discussed, the pre-

ferred cleavage plane changes as carbon is depleted from $\{100\}$ to $\{111\}$. The changes are significant, causing a doubling of the $\{100\}$ surface energy and causing the $\{111\}$ surface energy to drop to 42% of its original value. The effects on the $\{110\}$ plane are modest, hardly changing between the carbon filled and the carbon-depleted forms. These trends are important to keep in mind because they will actually carry to the other tantalum carbide structures, like the C6 structured α -Ta₂C.

3.2 | Effect of carbon depletion in cleavage fracture in α -Ta₂C

Cleavage in α -Ta₂C is more complicated that TaC due to its lower symmetry. However, to start to understand anisotropy and chemistry effects on cleavage, we first examine cleavage along the basal planes, which are close-packed planes just like the {111} planes in TaC. α -Ta₂C has the C6 structure, which is comprised a hcp stacking of the metal atoms with the carbon atoms filling alternating layers of the octahedral interstices. This results in two types of cleavage planes, those that separate metal and carbon atoms, M–X, and those that separate metal and metal atoms, M–M. These values and the planes are shown in Figure 5A. The absence of carbon, which would otherwise contribute to covalent bonding, leads to a structurally weaker plane that requires less energy to fracture.

Figure 5B shows the cleavage energies as a function of both carbon depletion and addition within these basal planes. For the M–M plane, we added carbon and note that the cleavage energy increased, as expected. Furthermore, removal of carbon form the M–X plane causes the cleavage energy to decrease. It is also interesting to note that the two planes are different in more than just chemistry because the fully carbon-depleted layers and fully carbon populated planes have different cleavage energy is dependent on more than the nearest neighbor chemical bonds.

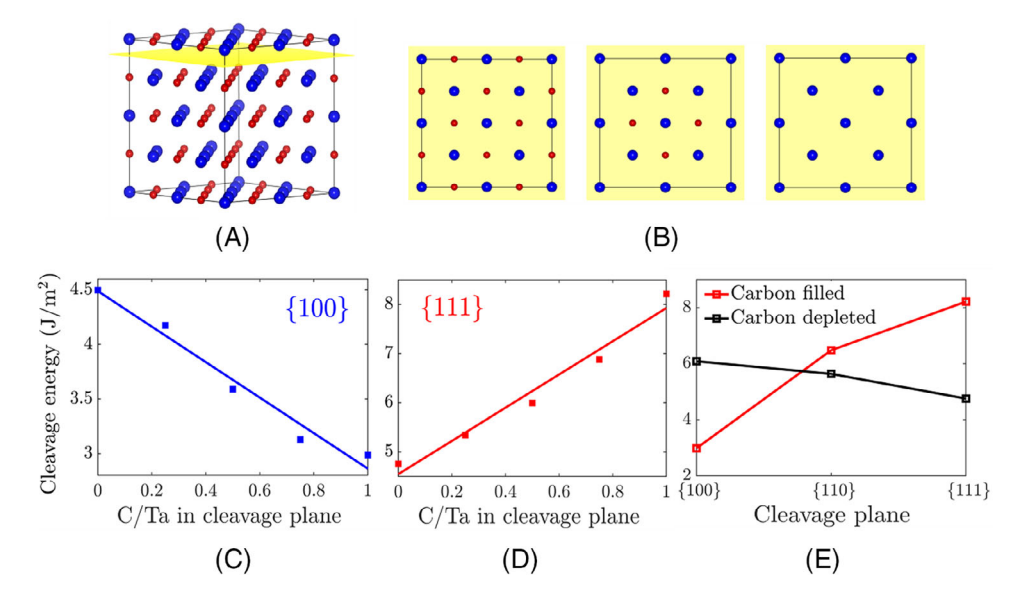


FIGURE 4 The effects of carbon depletion on the cleavage energy of B1 TaC_x . (A) The cleavage plane was increases in the two periodic directions normal to the cleavage plane as shown. (B) The carbon on both sides of the planes was systematically deleted to create the desired fracture plane stoichiometry. (C) The cleavage energy on the {100} plane and (D) {111} planes as a function of carbon content. (E) The cleavage energy for the three low index planes for completely carbon filled and completely carbon-depleted chemistries.

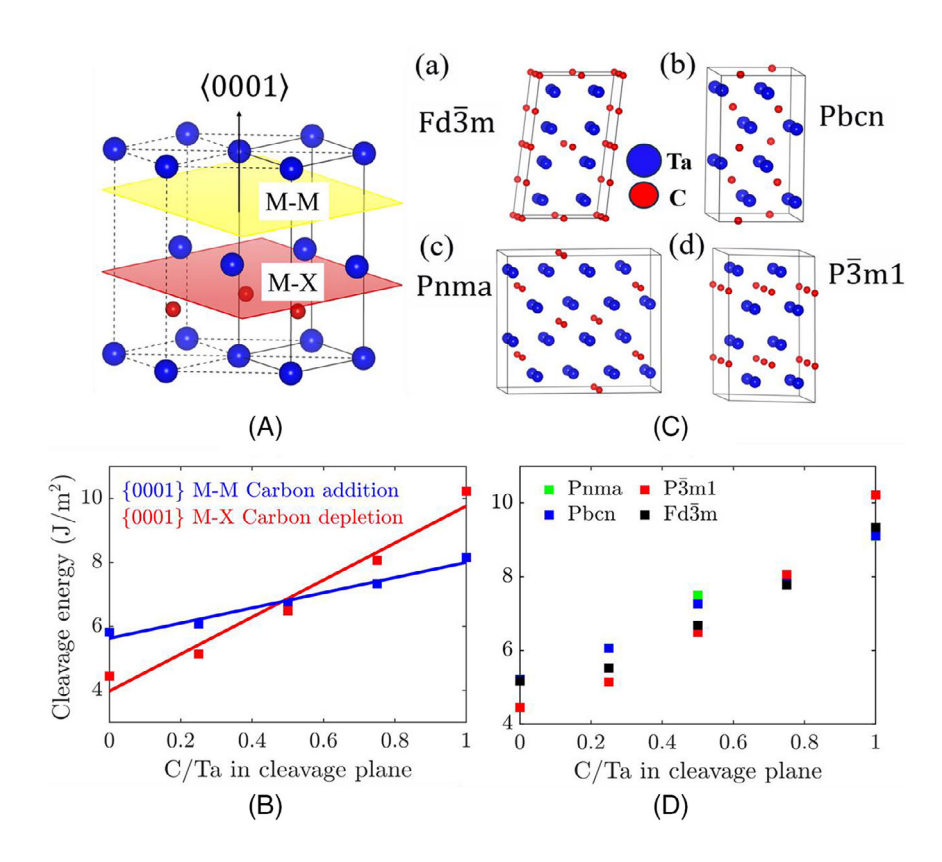
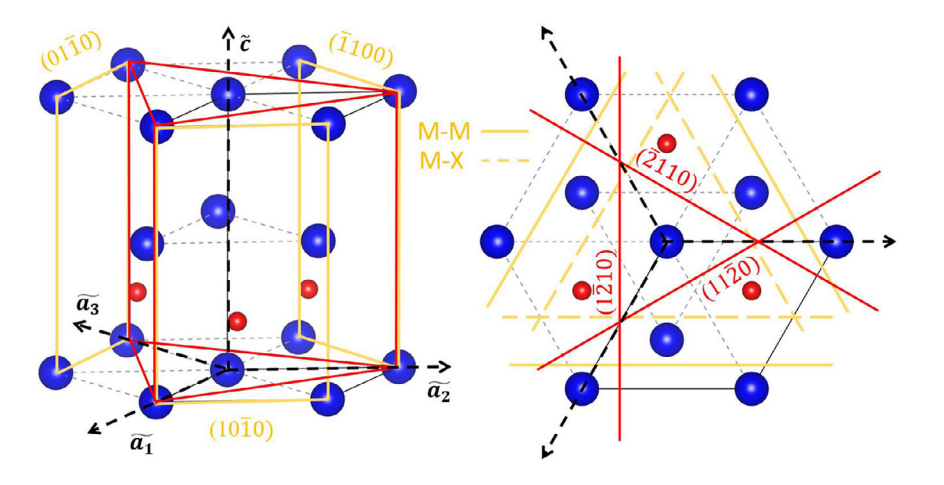


FIGURE 5 The cleavage energy of the close-packed planes in Ta₂C. (A) The cleavage energy of the two chemically distinct basal planes, M–M and M–X, the M–M bonded planes have lower cleavage energy. (B) The change in cleavage energy on these two planes as a function of carbon composition. (C) Other M₂C structures whose close-packed planes only have a single chemistry, which is MC_{0.5}. (D) The variation of the cleavage energy of these other close-packed planes plotted as a function of chemistry.

To further explore the impact of carbon atom ordering on cleavage energy, we simulated cleavage fractures in the close-packed planes of various vacancy-ordered M_2C structures. These additional structures are illustrated in Figure 5C, and differ from α -Ta₂C only by carbon atom ordering; except for the Fd $\bar{3}$ m which has a fcc metal atom

stacking sequence. The results of the cleavage energy are shown in Figure 5D, which include the removal and addition of carbon to the cleavage plane. The nondefected structures have only one type of close-packed plane and this occurs at the C/Ta=0.5 ratio. These results demonstrate that the cleavage energy is roughly independent of



metal atom ordering (fcc vs. hcp) and the specific details of carbon atom ordering. These results would be particularly representative of the high temperature L'3 structured Ta_2C , β - Ta_2C .

Collectively, these results indicate that ordered C6 α -Ta₂C can have a modest cleavage energy of 4.5–6 J/m², on the carbon vacant {0001} planes (M–M), as would any structure whose close-packed planes have one that is carbon depleted. The L'3 Ta₂C structure would likely have a higher cleavage energy of 7 J/m². Nevertheless, the significance of these cleavage energies must be cast relative to the other cleavage energies in these structures.

3.3 | Fracture along different cleavage planes in α -Ta₂C

In order to establish what the cleavage energy of the nonbasal planes is for comparison, we investigated cleavage fracture along the pyramidal and prismatic planes. There are two families of prismatic planes: {1120} and {1100} (Figure 6) with three planes per family. The {11\bar{2}0} cleavage plane has only one type of chemical configuration with each plane having a TaC_{0.5} composition and the planes are evenly spaced at 1.6 Å as shown in Figure 6; and the cleavage energy we found is 7.02 J/m². The other prismatic plane, the $\{\bar{1}100\}$, has two chemical configurations: M–M and M–X. However, the M–M configuration only has a slightly lower cleavage energy at 7.29 J/m² compared to 7.77 J/m². Notably, both configurations having an identical interplanar spacing of 0.9 Å and cutting these planes cuts both M-M and M-X bonds regardless of the atoms directly across the planes.

The first pyramidal planes we considered are the same investigated by Wang et al.³⁰ due to their low indices, which are shown in Figure 7A,B. There are two distinct families of these low index pyramidal planes: $\{\bar{1}101\}$ and $\{1\bar{1}01\}$. Both of these pyramidal planes have two chemical

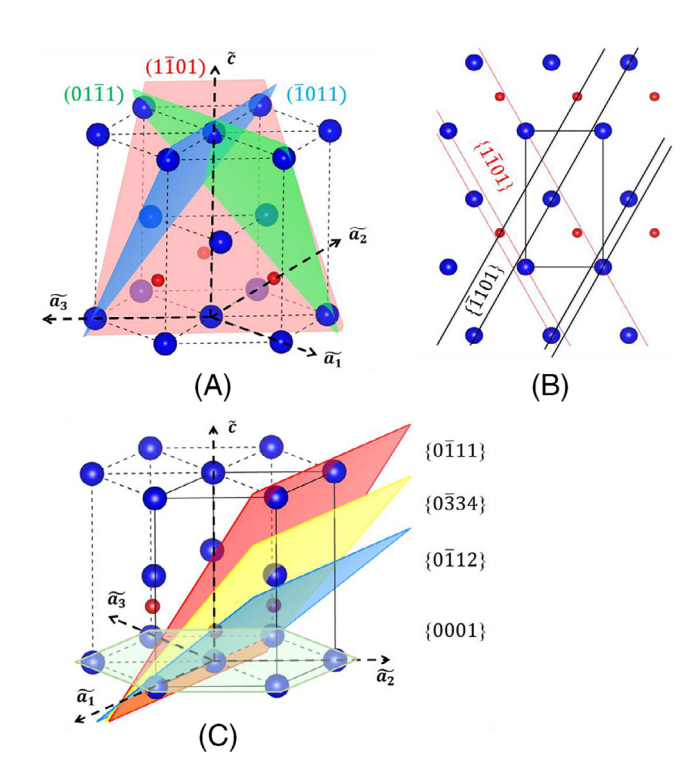


FIGURE 7 The pyramidal planes in α -Ta $_2$ C examined in this work. (A) The threefold symmetry of C6 α -Ta $_2$ C results in three planes in each family with the three $\{1\bar{1}01\}$ planes shown here. (B) In addition, the trigonal nature results in the $\{1\bar{1}01\}$ and $\{\bar{1}101\}$ pyramidal planes in α -Ta $_2$ C being different planes with different chemistries and interatomic placing. (C) The progression of pyramidal planes between the $\{0\bar{1}10\}$ and $\{0001\}$ planes.

variants which are labeled M–M and M–X as shown in Figure 7A,B. For the $\{\bar{1}101\}$, the M–M configuration has a cleavage energy of 8.69 J/m² while the M–X has a cleavage energy of 7.56 J/m². For the $\{1\bar{1}01\}$, the larger spaced M–M planes have a cleavage energy of 5.07 J/m² and the very small spaced M–X planes have a cleavage energy of 8.87 J/m². This might seem surprising because Wang et al.³⁰ found this plane to have a very high generalized



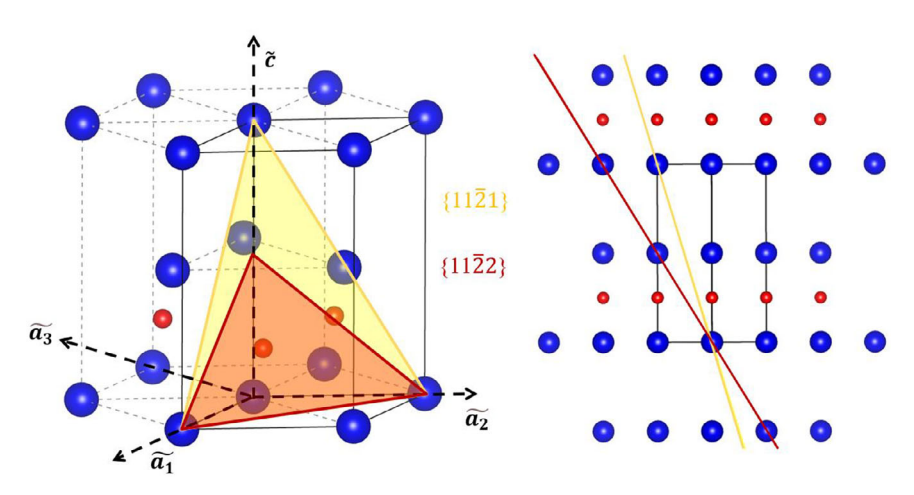


FIGURE 8 The $\{11\bar{2}1\}$ and $\{11\bar{2}2\}$ pyramidal planes in α -Ta₂C. These pyramidal planes lie between the $\{11\bar{2}0\}$ and $\{0001\}$ planes.

stacking fault energy, the difference here is that we are not sliding atomic planes but separating them. What is even more interesting is that this energy is lower than cleavage of the M–M basal plane. This means that the basal planes are not the lowest cleavage energy plans in α -Ta₂C.

Similar to our examination of cleavage in the B1 structure, we also examined how the cleavage energy changes as a function of the angle the pyramidal plane makes with the basal plane, transitioning from $\{0\overline{1}10\}$ to $\{0001\}$ as shown in Figure 7C. This includes the new pyramidal planes {0334} with cleavage energy of 5.45 J/m² and {0112} with cleavage energy of 5.90 J/m². The cleavage energy of the planes in Figure 7C order from least to greatest as: $\{0\bar{3}34\} < \{0001\} < \{0\bar{1}12\} < \{0\bar{1}10\}$. Again, we see that the lowest energy is not the basal plane, but on the {0334} plane. Another plane, the {0332}, also has a low cleavage energy of 5.98 J/m². The conjugate planes of the {0334} and {0332} have relatively higher cleavage energies of 7.57 J/m^2 and 7.97 J/m^2 , respectively. This indicates that there are many low cleavage energy planes in C6 α -Ta₂C.

To finish our examination of the pyramidal planes, we examine those that contain the $\langle 11\bar{2}0 \rangle$ as shown in Figure 8. These include the $\{11\bar{2}1\}$, $\{11\bar{2}\bar{1}\}$, $\{11\bar{2}2\}$, and $\{11\bar{2}\bar{2}\}$ planes. The $\{11\bar{2}1\}$ cleavage planes have M–M and M–X compositions and have similar cleavage energies of around 7 J/m^2 . The $\{11\bar{2}2\}$ has a single composition plane and slightly lower cleavage energy 6.88 J/m². However, none of these pyramidal planes showed energies that were below the low value of 6 J/m^2 .

We found a large number of moderate-energy cleavage planes in $\alpha\text{-}\mathrm{Ta_2}\mathrm{C}$ —the basal {0001} M–M and three families of pyramidal planes, which all exhibit cleavage energies ranging from 5 to 6 J/m² (Table 1). The abundance of these moderate-energy cleavage planes suggests that $\alpha\text{-}\mathrm{Ta_2}\mathrm{C}$ has multiple potential pathways for crack propagation. All of these planes have the potential to act as paths for crack propagation, limiting the ability of the structure

to have crack deflection, and crack bridging. This raises the question of whether this is true in the zeta phase as well.

3.4 | Fracture anisotropy in ζ -Ta₄C₃, ζ -Ta₃C₂, and η -Ta₃C₂

Previous reports of fracture in the zeta phase indicate that the M–M {0001} plane has the lowest cleavage energy. 10,29 However, our results in Ta₂C suggest that there may be other competitive cleavage planes. Furthermore, recent work has demonstrated that zeta phase is actually chemically the ζ -Ta₃C₂, 19 which has never been examined from a fracture perspective. Thus, in this section we examine the previous ζ -Ta₄C₃ structure, the new ζ -Ta₃C₂ and the related η -Ta₃C₂ structure to better understand how the stacking sequences, carbon atom ordering, and chemistry affect fracture. Notably, it is critical to understand if the M–M {0001} is the lowest energy cleavage plane or if there are others similar to Ta₂C.

The cleavage energy of select planes in the ζ -Ta₄C₃ structure is shown in Figure 9. The cleavage energy for the $\{0001\}$ M–M configuration is 5.17 J/m². For the M–X plane, we selected one of the three reported by Yan et al. ¹⁰ and found a value of 10.82 J/m², which lies in their reported range of 8–11 J/m². Thus, our results are in agreement with previous investigations ^{10,29} and demonstrate the preference for cleavage on the M–M variant of the $\{0001\}$ planes.

A thorough examination of all the pyramidal planes in any of these structures would take substantial time and resources and thus we narrowed our examination to on planes that we hypothesize to exhibit low cleavage energy, analogous to those identified in the α -Ta₂C structure. Notably, the $\{0\bar{1}18\}$ looks similar to the $\{0\bar{3}34\}$ in Ta₂C and the $\{001\}$ in TaC, both of which have low cleavage energy. This plane indeed does have a low cleavage energy: 4.23 J/m², contradicting the previously accepted

TABLE 1 Cleavage energies in different planes of α -Ta₂C.

	0 0	-	-			
	Planes	Туре	Cleavage energy (J/m²)	Planes	Туре	Cleavage energy (J/m²)
Basal	{0001}	M-M	5.82	{0001}	M-X	10.21
Prismatic	$\{\bar{1}100\}$	M-M	7.29	$\{11\bar{2}0\}$		7.02
		M-X	7.77			
Pyramidal	$\{\bar{1}101\}$	M-M	8.69	$\{1\bar{1}01\}$	M-M	5.07
		M-X	7.56		M-X	8.87
	$\{0\bar{1}12\}$		5.90	$\{01\bar{1}2\}$		7.47
	$\{11\bar{2}2\}$		6.88	$\{11\bar{2}1\}$	M-M	7.22
					M-X	7.12
	{0334}		5.45	{0334}		7.57
	{0332}		5.98	{0332}		7.97

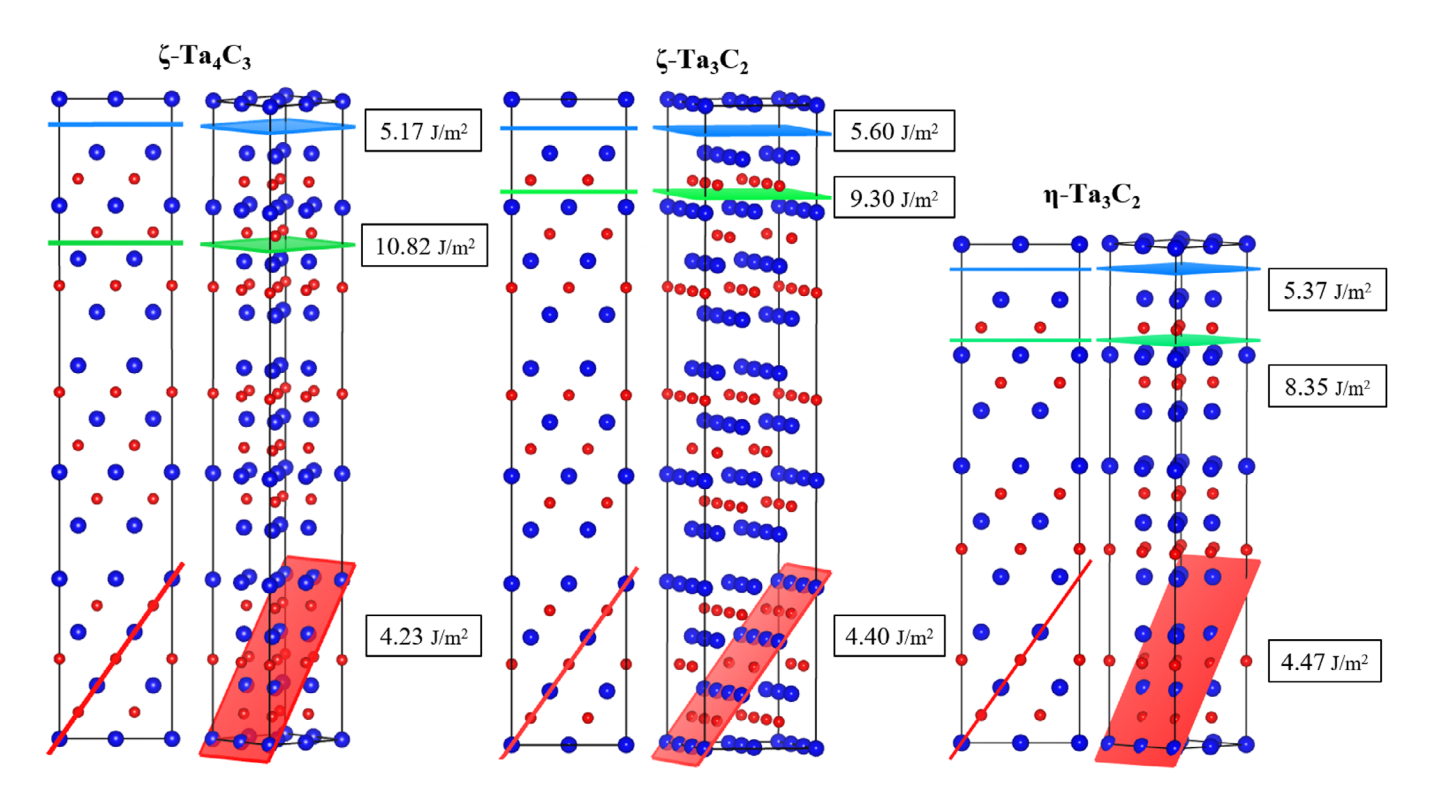


FIGURE 9 The fracture planes and cleavage energy in the zeta (ζ) and eta phases (η) of tantalum carbide.

view that the basal {0001} M-M plane has the lowest cleavage energy. 10,29

In ζ -Ta₃C₂ (C2/m), the {001} M–M configuration shows a cleavage energy of 5.60 J/m², and the M–X configuration is higher at 9.30 J/m². Notably, the {014} plane exhibits the lowest cleavage energy at 4.40 J/m². The cleavage energies for the {0001} basal plane configurations in η -Ta₃C₂ are 5.37 J/m² for M–M and 8.35 J/m² for M–X, while the cleavage energy for the {0116} plane is 4.47 J/m². This indicates that the stacking sequence or changes in chemistry does not affect the cleavage energies of these planes considerably.

These results demonstrate that there are at least four easy cleavage planes in ζ -Ta₄C₃ (three $\{0\bar{1}18\}$ and one $\{0001\}$ M–M) and similar easy cleavage planes in ζ -Ta₃C₂. Here, we define the easy cleavage planes having cleavage energies within 1 J/m² relative to the lowest energy plane. For comparison, the low number of low-energy cleavage planes in TaC is three, the $\{001\}$ planes, with possibly the $\{014\}$ being low cleavage energy as well. In the Ta₂C structure, we see that there are many equally low cleavage energy planes. This suggests that α -Ta₂C and the ζ -Ta₄C_{3-x} are not more anisotropic in regard to fracture than γ -TaC.

The observation that TaC does not have any more easy cleavage planes, and arguably less, compared to the zeta phase and Ta₂C is an important finding. This is because toughening in the presence of the zeta phase shows high fracture toughness and a rising R-curve, indicative of microstructural toughening. One posited explanation for this is the preference for cleavage on the carbon-depleted basal planes of the zeta phase. 5,16-21 This would create the preferential cleavage seen in experiments^{5,9} and crack deflection around unfavorably oriented grains would cause grain bridging. However, these results contradict the notion that easy cleavage occurs only on these planes. This further suggests that a preference for cleavage on these planes and the associated toughening may be due to localized preferred plasticity. Easy slip has been observed along the Ta-Ta basal planes in Ta₄C₃⁵ and Ta₂C, ³⁰ can induce delamination⁷ and explain the preference for cleavage on these close-packed planes.

4 | SUMMARY AND CONCLUSION

In this study, we investigated the anisotropy of cleavage energy in the tantalum carbides in order to better understand the high fracture toughness of the zeta phase (ζ -Ta₄C_{3 - x}), which has toughness values ranging from 11 to 15 MPa \sqrt{m}^{5-7} compared to 4–6 MPa $\sqrt{m}^{5,8,11-13}$ for cubic γ -TaC and 6–9 MPa $\sqrt{m}^{5,8,9,14,15}$ for α -Ta₂C. Our objective was to elucidate the underlying reasons for the exceptional fracture toughness observed in the zeta phase, employing DFT to calculate cleavage energies across various crystallographic planes of these compounds.

In stoichiometric TaC, the {100} planes are the lowest cleavage energy planes. The cleavage energy of these planes goes up with carbon loss, while the cleavage energy of the {111} planes decreases, eventually making the {111} planes more favorable for fracture.

The M–M variant of the $\{0001\}$ basal planes in α -Ta $_2$ C has a low cleavage energy, but they do not have the lowest cleavage energy. The lowest energy cleavage plane is pyramidal $\{0\bar{3}34\}$ plane. Other pyramidal planes, $\{0\bar{3}\bar{3}2\}$ and $\{1\bar{1}02\}$ also have low cleavage energies. This makes the fracture of Ta $_2$ C to be quite isotropic with many cleavage planes for a crack to follow.

In the zeta phase, we discovered similar low-energy cleavage planes across the previously acknowledged $\zeta\textsc{-}\mathrm{Ta}_4C_3$ structure of zeta phase, the actual thermodynamically stable $\zeta\textsc{-}\mathrm{Ta}_3C_2$ structure, and the related $\eta\textsc{-}\mathrm{Ta}_3C_2$ structure. Our findings on these structures indicate that the stacking sequences and carbon atom ordering have little effect on cleavage fracture anisotropy. Furthermore, the presence of multiple low-energy cleavage planes in zeta phase implies that fracture anisotropy within tantalum

carbides is not significantly different across the studied compounds: TaC, α - Ta_2C , and the ζ - Ta_3C_2 .

The abundance of multiple low cleavage energy planes means there are multiple fracture pathways which facilitates crack deflection during propagation. However, this also implies a reduced dependency on grain orientation for fracture propagation, potentially diminishing the effectiveness of grain bridging as a toughening mechanism. In experiments, 5,9 the preference of cleavage has been observed along the carbon-depleted basal planes only, not along the other low-energy cleavage planes that we have found. This suggests that the preference for certain cleavage planes cannot be solely attributed to cleavage energy values. Localized plastic deformation might play a key role in the preference of particular cleavage plane and also might be responsible for other toughening mechanism like delamination.

ACKNOWLEDGMENTS

This material is based upon work supported by the National Science Foundation under grant numbers 2323458 and 2323456. This work utilized the Alpine high performance computing resource at the University of Colorado Boulder. Alpine is jointly funded by the University of Colorado Boulder, the University of Colorado Anschutz, Colorado State University, and the National Science Foundation (award no. 2201538). Any opinions, findings, and conclusions or recommendations expressed in this material are those of the author(s) and do not necessarily reflect the views of the National Science Foundation.

ORCID

Sajjad Hossain https://orcid.org/0009-0009-3213-8614 Christopher R. Weinberger https://orcid.org/0000-0001-9550-6992

REFERENCES

- Toth L. Transition metal carbides and nitrides. Elsevier, New York and London (1971).
- Wuchina E, Opila E, Opeka M, Fahrenholtz B, Talmy I. UHTCs: ultra-high temperature ceramic materials for extreme environment applications. Electrochem Soc Interface. 2007;16(4):30. https://doi.org/10.1149/2.F04074IF
- Pierson HO. Handbook of refractory carbides and nitrides: properties, characteristics, processing, and applications. Park Ridge, NJ: Noyes Publications; 1996
- Thompson GB, Weinberger CR. Tantalum carbides: their microstructures and deformation behavior. In: Fahrenholtz WG, Wuchina EJ, Lee WE, Zhou Y, editors. Ultra-high temperature ceramics. Hoboken, NJ: John Wiley & Sons, Inc; 2014. p. 291–315. https://doi.org/10.1002/9781118700853.ch12
- 5. Schulz BC, Lee H, Mogilevsky P, Weinberger CR, Parthasarathy TA, Matson LE, et al. Experimental investigation into the crack

journal

- propagation in multiphase tantalum carbide ceramics. Mater Sci Eng. 2017;695:315-21. https://doi.org/10.1016/j.msea.2017.04.043
- 6. Limeng L, Feng Y, Yu Z, Zhiguo Z. Microstructure and mechanical properties of spark plasma sintered TaC0.7 ceramics: rapid communications of the American Ceramic Society. J Am Ceram Soc. 2010;93(10):2945-47. https://doi.org/10.1111/j.1551-2916.2010.03908.x
- 7. Schwind EC, Fahrenholtz B, Watts J, Hilmas G. Effect of ζ-Ta₄C_{3-x} on the mechanical properties of tantalum carbide at elevated temperatures. J Am Ceram Soc. 2022;105(12):7625-34. https://doi.org/10.1111/jace.18692
- 8. Hackett K, Verhoef S, Cutler RA, Shetty DK. Phase constitution and mechanical properties of carbides in the Ta-C system. J Am Ceram Soc. 2009;92(10):2404-7. https://doi.org/10.1111/j. 1551-2916.2009.03201.x
- 9. Sygnatowicz M, Cutler RA, Shetty DK. ζ-Ta₄C_{3-x}: a high fracture toughness carbide with rising-crack-growth-resistance (R-curve) behavior. J Am Ceram Soc. 2015;98(8):2601–8. https:// doi.org/10.1111/jace.13635
- 10. Yan WL, Sygnatowicz M, Lu GH, Liu F, Shetty DK. Firstprinciples study on surface stability of tantalum carbides. Surf Sci. 2016;644:24-28. https://doi.org/10.1016/j.susc.2015.09.003
- 11. Rowcliffe DJ, Hollox GE. Plastic flow and fracture of tantalum carbide and hafnium carbide at low temperatures. J Mater Sci. 1971;6(10):1261-69. https://doi.org/10.1007/BF00552039
- 12. Rowcliffe DJ, Warren WJ. Structure and properties of tantalum carbide crystals. J Mater Sci. 1970;5(4):345-50. https://doi.org/ 10.1007/PL00020109
- 13. Song K, Xu Y, Zhao N, Shang Z, Shen L, Wang J. Evaluation of fracture toughness of tantalum carbide ceramic layer: a Vickers indentation method. J Mater Eng Perform. 2016;25(7):3057-64. https://doi.org/10.1007/s11665-016-2161-x
- 14. Alexandre N, Desmaison M, Valin F, Boncoeur M. Synthesis of high toughness tantalum carbide Ta₂C by HIP-reaction sintering. In: Delaey L, Tas H, editors. Hot isostatic pressing '93. Amsterdam: Elsevier; 1994. p. 443-50. https://doi.org/10.1016/ B978-0-444-89959-0.50053-0
- 15. Liu L, Liu H, Ye F, Zhang Z, Zhou Y. Microstructure and mechanical properties of the spark plasma sintered Ta₂C ceramics. Ceram Int. 2012;38(6):4707-13. https://doi.org/10.1016/j. ceramint.2012.02.055
- 16. Morris RA, Wang B, Butts D, Thompson GB. Variations in tantalum carbide microstructures with changing carbon content. Int J Appl Ceram Technol. 2013;10(3):540-51. https://doi.org/10. 1111/j.1744-7402.2012.02761.x
- 17. Morris RA, Wang B, Matson LE, Thompson GB. Microstructural formations and phase transformation pathways in hot isostatically pressed tantalum carbides. Acta Mater. 2012;60(1):139-48. https://doi.org/10.1016/j.actamat.2011.09.036
- 18. Yu XX, Weinberger CR, Thompson GB. Ab initio investigations of the phase stability in tantalum carbides. Acta Mater. 2014;80:341-49. https://doi.org/10.1016/j.actamat.2014.07.070
- 19. Weinberger CR, Thompson GB. A computational search for the zeta phase in the tantalum carbides. J Am Ceram Soc. 2019;102(3):1454-62. https://doi.org/10.1111/jace.15970
- 20. Weinberger CR, Thompson GB. Review of phase stability in the group IVB and VB transition-metal carbides. J Am Ceram Soc. 2018;101(10):4401-24. https://doi.org/10.1111/jace.15768

- 21. Yu XX, Weinberger CR, Thompson GB, Ab initio investigations of the phase stability in group IVB and VB transition metal carbides. Comput Mater Sci. 2016;112:318-26. https://doi.org/10. 1016/i.commatsci.2015.10.038
- 22. Schwind EC, Hilmas GE, Fahrenholtz WG. Thermal properties and elastic constants of ζ-Ta₄C_{3-x}. J Am Ceram Soc. 2020;103(5):2986-90. https://doi.org/10.1111/jace.16997
- 23. Schwind EC, Reece MJ, Castle E, Fahrenholtz WG, Hilmas GE. Thermal and electrical properties of a high entropy carbide (Ta, Hf, Nb, Zr) at elevated temperatures. J Am Ceram Soc. 2022;105(6):4426-34. https://doi.org/10.1111/jace.18400
- 24. Li Z, Shi F, Liu L, Vleugels J, Huang S. Effects of 20 mol% Fe, Co, Ni additions on phase formation, microstructure and mechanical properties of TaC_x (x = 0.5, 0.55, 0.6, 0.7) ceramics. Int J Refract Met Hard Mater. 2021;95:105436. https://doi.org/10.1016/ j.ijrmhm.2020.105436
- 25. Shi F, Li Z, Liu L, Wu J, Ma J, Wang Y. Stacking behavior of the close-packed Ta-atom planes and its effects on formation of "hybrid grains" in TaC_{0.66-0.7} ceramics. Ceram Int. 2020;46(11, Part B):19092-102. https://doi.org/10.1016/j.ceramint.2020.04.
- 26. Shi F, Liu L, Wang Y-J, Geng G. ζ-Ta₄C₃ lamellae growth behavior and its effects on microstructure and fracture toughness of TaC_{0.6}-Cu composites. J Alloys Compd. 2019;820:153175. https:// doi.org/10.1016/j.jallcom.2019.153175
- 27. Liu L, Vleugels J, Huang S, Wei J, Wang Y. Strengthened interfacial bonding and its effects on fracture mode of TaC ceramics with addition of B. J Eur Ceram Soc. 2020;40(4):1067-77. https:// doi.org/10.1016/j.jeurceramsoc.2019.12.013
- 28. Leipold MH, Nielsen TH. The mechanical behavior of tantalum carbide and magnesium oxide. Technical report 32-1201. Pasadena, CA: Jet Propulsion Laboratory, CIT; 1967.
- 29. Yu H, Thompson GB, Weinberger CR. The role of chemistry and bonding in regulating fracture in multiphase transition metal carbides and nitrides. Extreme Mech Lett. 2017;17:1-6. https:// doi.org/10.1016/j.eml.2017.09.004
- 30. Wang B, De Leon N, Weinberger CR, Thompson GB. A theoretical investigation of the slip systems of Ta₂C. Acta Mater. 2013;61(11):3914-22. https://doi.org/10.1016/j.actamat.2013.01. 047
- 31. Teague MC, Hilmas GE, Fahrenholtz WG. Mechanical properties of reactively processed W/Ta2C-based composites. J Eur Ceram Soc. 2010;30(11):2197-201. https://doi.org/10.1016/j. jeurceramsoc.2010.02.006
- 32. Becher PF. Microstructural design of toughened ceramics. J Am Ceram Soc. 1991;74(2):255-69. https://doi.org/10.1111/j.1151-2916. 1991.tb06872.x
- 33. Brizes WF, Tobin JM. Isolation of the zeta phase in the system tantalum-carbon. J Am Ceram Soc. 1967;50(2):115-16. https:// doi.org/10.1111/j.1151-2916.1967.tb15055.x
- 34. Griffith AA, Taylor GI. The phenomena of rupture and flow in solids. Philos Trans R Soc Lond Ser A. 1997;221(582-593):163-98. https://doi.org/10.1098/rsta.1921.0006
- 35. Yu H, Guziewski M, Thompson GB, Weinberger CR. A model for understanding the formation energies of nanolamellar phases in transition metal carbides and nitrides. Model Simul Mater Sci Eng. 2016;24(5):055004. https://doi.org/10.1088/0965-0393/24/5/ 055004



- 36. Weinberger CR, Yu H, Wang B, Thompson GB. A computational investigation into the microstructures and stability of the zeta phase in transition metal carbides and nitrides. Adv Appl Ceram. 2018;117(Suppl 1):s26–s33. https://doi.org/10.1080/17436753.2018.1510818
- 37. Santoro G, Probst HB. An explanation of microstructures in the tantalum-carbon system. Adv X-Ray Anal. 1963;7:126–35. https://doi.org/10.1154/S0376030800002469
- 38. Santoro G. Variation of some properties of tantalum carbide with carbon content(Variation in tensile strength, bending, color, and diamagnetic properties of tantalum carbide with carbon content). Trans Metall Soc AIME. 1963;227:1361–68.
- 39. Wiesenberger H, Lengauer W, Ettmayer P. Reactive diffusion and phase equilibria in the V-C, Nb-C, Ta-C and Ta-N systems. Acta Mater. 1998;46(2):651-66. https://doi.org/10.1016/S1359-6454(97)00204-8
- Zaplatynsky I. Observations on zeta phase in the system Ta-C. J Am Ceram Soc. 1966;49(2):109–109. https://doi.org/10.1111/ i.1151-2916.1966.tb13223.x
- 41. Gusev AI, Kurlov AS, Lipatnikov VN. Atomic and vacancy ordering in carbide ζ -Ta4C_{3-x} (0.28 \leq x \leq 0.40) and phase equilibria in the Ta-C system. J Solid State Chem. 2007;180(11):3234–46. https://doi.org/10.1016/j.jssc.2007.09.015
- 42. Yvon K, Parthé E. On the crystal chemistry of the close-packed transition-metal carbides. I. The crystal structure of the ζ-V, Nb and Ta carbides. Acta Crystallogr B Struct Crystallogr Cryst Chem. 1970;26(2):149–53. https://doi.org/10.1107/S0567740870002091
- 43. Martin JL, Rocher A, Jouffrey B, Costa P. Electron diffraction patterns of the (Ta, C) ζ phase. Philos Mag. 1971;24(192):1355–64. https://doi.org/10.1080/14786437108217417
- 44. Gusev AI, Lipatnikov VN. Ordering in the ζ -Ta₄C_{3--x} carbide phase. Jetp Lett. 2005;82(5):287–91. https://doi.org/10.1134/1.2130914
- 45. Zhao X, Togaru M, Guo Q, Weinberger CR, Lamberson L, Thompson GB. Carbon influence on fracture toughness of nio-bium carbides. J Eur Ceram Soc. 2019;39(16):5167–73. https://doi.org/10.1016/j.jeurceramsoc.2019.08.022
- Nieto A, Bisht A, Lahiri D, Zhang C, Agarwal A. Graphene reinforced metal and ceramic matrix composites: a review. Int Mater Rev. 2017;62(5):241–302. https://doi.org/10.1080/09506608.2016. 1219481
- 47. Kresse G, Hafner J. *Ab initio* molecular dynamics for liquid metals. Phys Rev B. 1993;47(1):558–61. https://doi.org/10.1103/PhysRevB.47.558
- Kresse G, Hafner J. Norm-conserving and ultrasoft pseudopotentials for first-row and transition elements. J Phys: Condens Matter. 1994;6(40):8245–57. https://doi.org/10.1088/0953-8984/6/40/015
- 49. Kresse G, Furthmüller J. Efficiency of ab-initio total energy calculations for metals and semiconductors using a plane-wave basis set. Comput Mater Sci. 1996;6(1):15–50. https://doi.org/10. 1016/0927-0256(96)00008-0
- 50. Kresse G, Furthmüller J. Efficient iterative schemes for *ab initio* total-energy calculations using a plane-wave basis set. Phys

- Rev B. 1996;54(16):11169–86. https://doi.org/10.1103/PhysRevB. 54.11169
- Blöchl PE. Projector augmented-wave method. Phys Rev B. 1994;50(24):17953-79. https://doi.org/10.1103/PhysRevB.50. 17953
- 52. Perdew JP, Burke K, Ernzerhof M. Generalized gradient approximation made simple. Phys Rev Lett. 1996;77(18):3865–68. https://doi.org/10.1103/PhysRevLett.77.3865
- Hugosson HW, Eriksson O, Jansson U, Ruban AV, Souvatzis P, Abrikosov IA. Surface energies and work functions of the transition metal carbides. Surf Sci. 2004;557(1):243–54. https://doi. org/10.1016/j.susc.2004.03.050
- 54. Li H, Zhang L, Zeng Q, Guan K, Li K, Ren H, et al. Structural, elastic and electronic properties of transition metal carbides TMC (TM = Ti, Zr, Hf and Ta) from first-principles calculations. Solid State Commun. 2011;151:602–6. https://doi.org/10.1016/j.ssc.2011.02.005
- 55. Galanakis I, Papanikolaou N, Dederichs PH. Applicability of the broken-bond rule to the surface energy of the fcc metals. Surf Sci. 2002;511(1–3):1–12. https://doi.org/10.1016/S0039-6028(02)01547-9
- Wynblatt P, Chatain D. Surface segregation anisotropy and the equilibrium shape of alloy crystals. Rev Adv Mater Sci. 2009;21(1):44–56.
- 57. Wang SG, Tian EK, Lung CW. Surface energy of arbitrary crystal plane of bcc and fcc metals. J Phys Chem Solids. 2000;61(8):1295–300. https://doi.org/10.1016/S0022-3697(99)00415-1
- Scheiber D, Pippan R, Puschnig P, Romaner L. Ab initio calculations of grain boundaries in bcc metals. Model Simul Mater Sci Eng. 2016;24(3):035013. https://doi.org/10.1088/0965-0393/24/3/035013
- 59. Sarochawikasit R, Wang C, Kumam P, Beladi H, Okita T, Rohrer GS, et al. Grain boundary energy function for α iron. Materialia. 2021;19:101186. https://doi.org/10.1016/j.mtla.2021.101186
- Wang K, Zhang W, Xu J, Dan W. The impact of misorientation on the grain boundary energy in bi-crystal copper: an atomistic simulation study. J Mol Model. 2022;28(2):47. https://doi.org/10. 1007/s00894-022-05037-7

SUPPORTING INFORMATION

Additional supporting information can be found online in the Supporting Information section at the end of this article.

How to cite this article: Hossain S, Thompson GB, Weinberger CR. Exploring fracture anisotropy in tantalum carbide compounds: A density functional theory approach. J Am Ceram Soc. 2024;1–12. https://doi.org/10.1111/jace.19917